SUPPLEMENTAL FIGURES

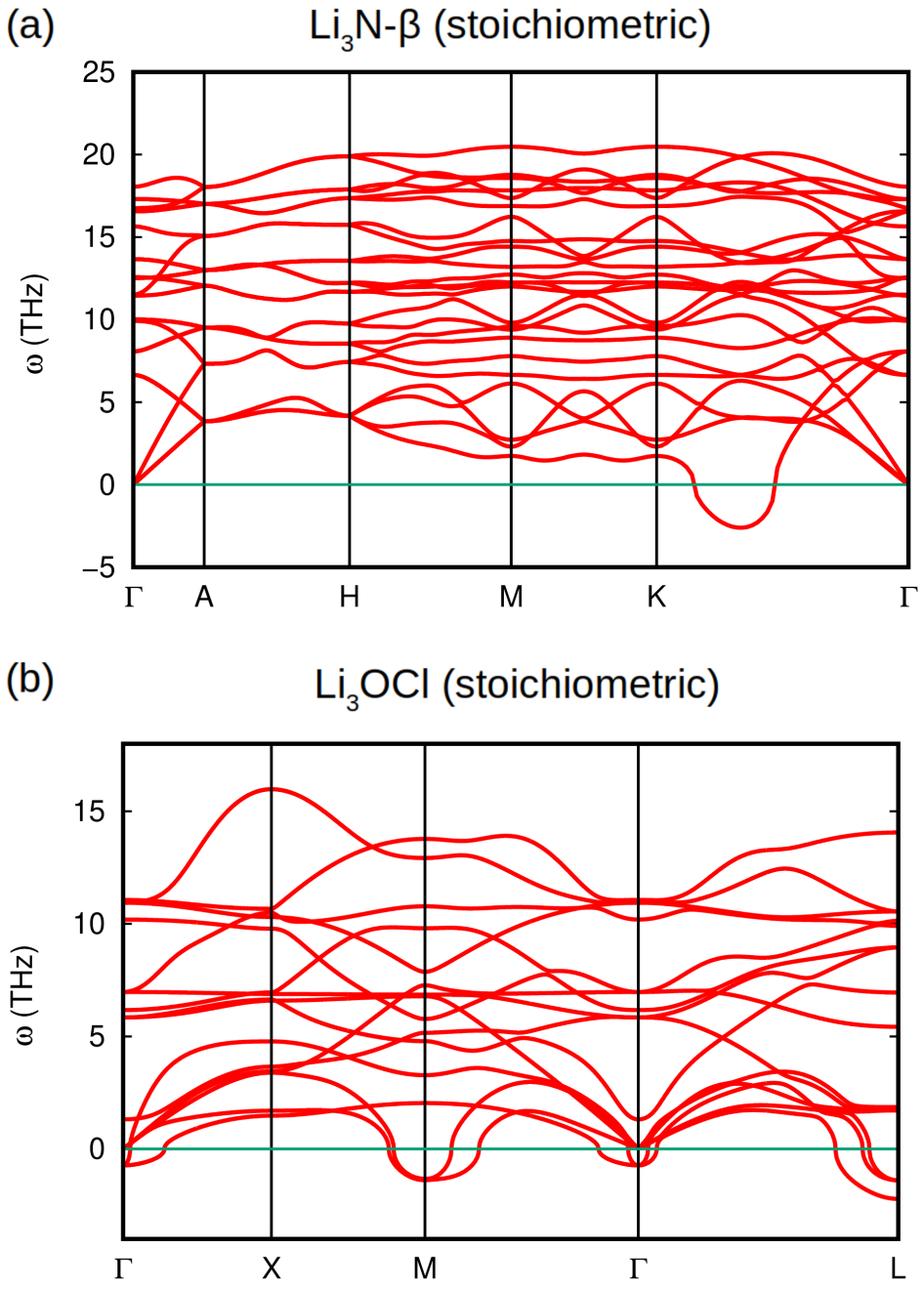

Supplemental Figure 1: Phonon spectrum of stoichiometric (a) Li_3N and (b) Li_3OCl calculated with zero-temperature harmonic approaches. The presence of imaginary phonon frequency modes are appreciated in both cases.

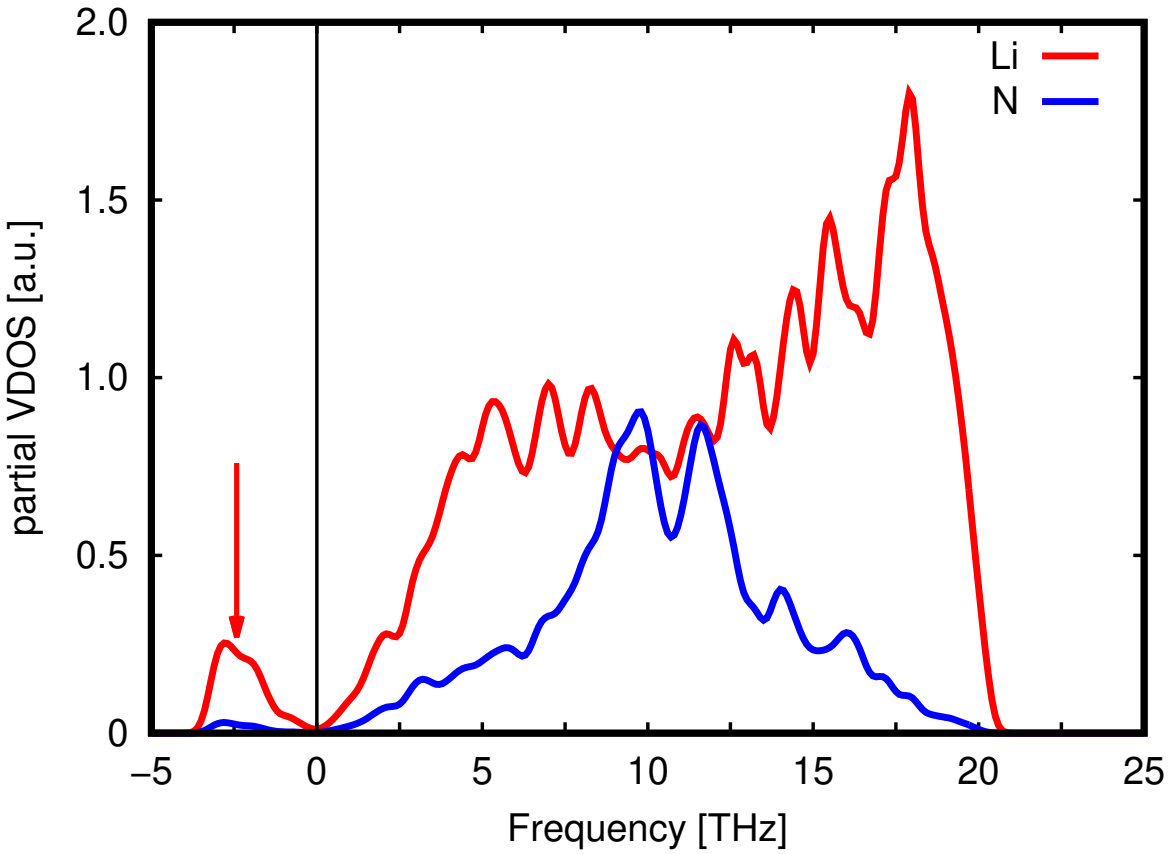

Supplemental Figure 2: Partial density of vibrational states calculated for non-stoichiometric Li_3N with zero-temperature harmonic approaches. The imaginary phonon frequency modes that appear (indicated by a red arrow) are mostly dominated by lithium ions.

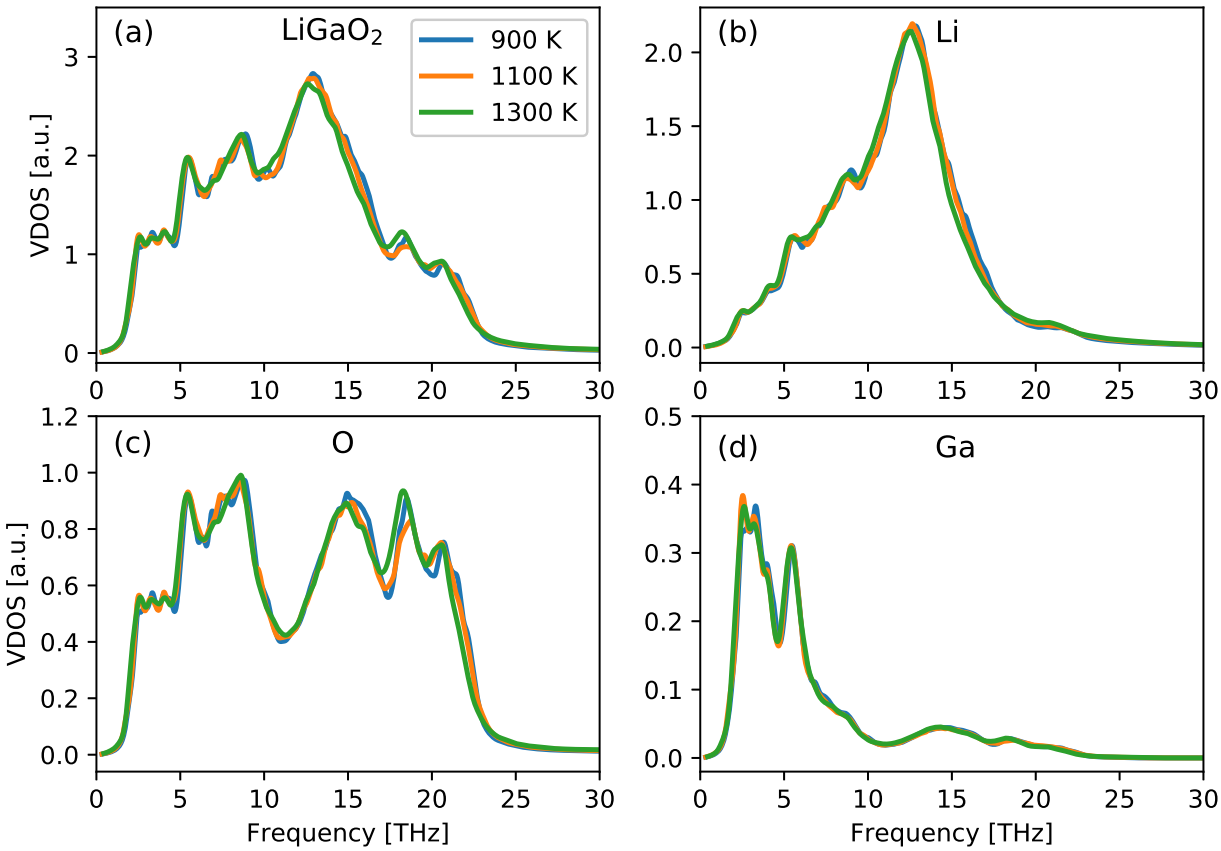

Supplemental Figure 3: Density of vibrational states calculated for non-stoichiometric $LiGaO_2$ at different temperatures by considering (a) all the atoms in the system and (b)-(d) each individual species. Results are obtained from the Fourier transform of the velocity-velocity autocorrelation function calculated during long AIMD simulations.

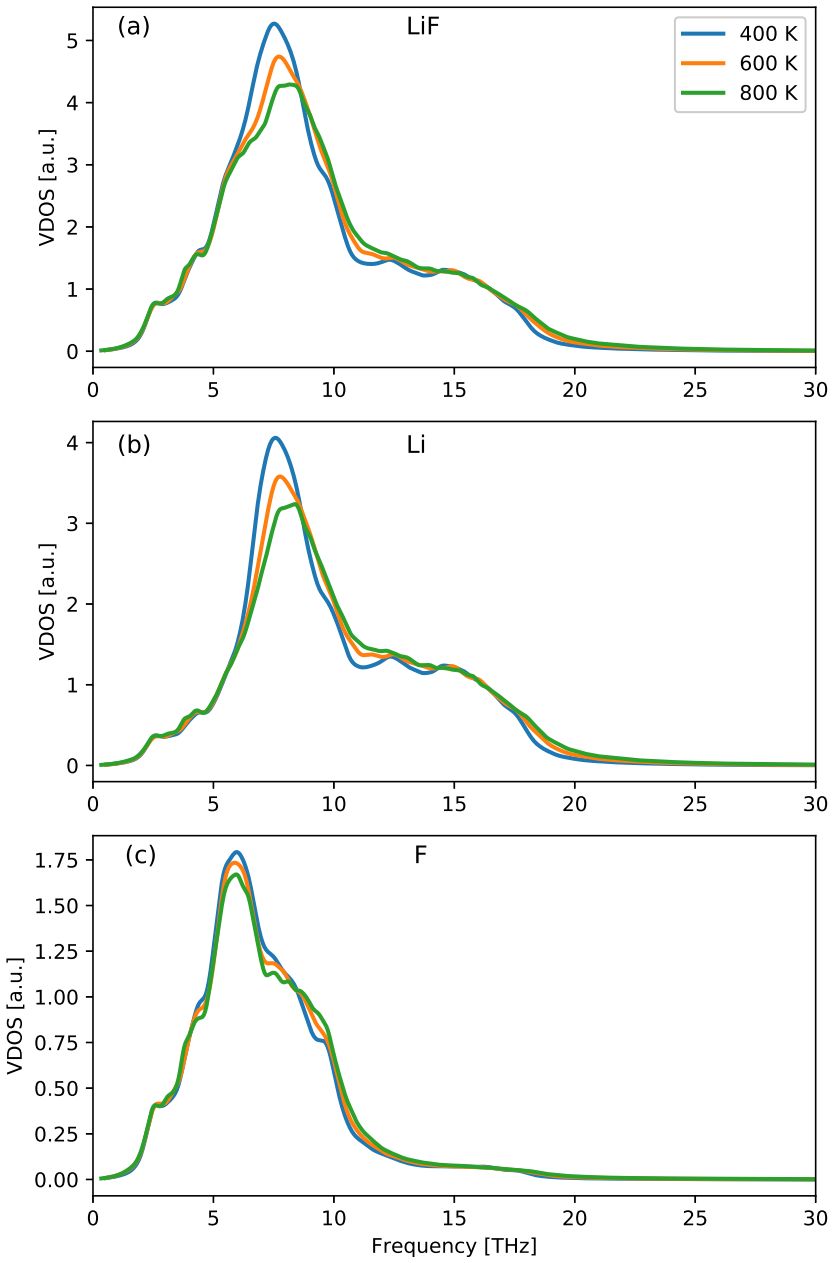

Supplemental Figure 4: Density of vibrational states calculated for non-stoichiometric LiF at different temperatures by considering (a) all the atoms in the system and (b)-(c) each individual species. Results are obtained from the Fourier transform of the velocity-velocity autocorrelation function calculated during long AIMD simulations.

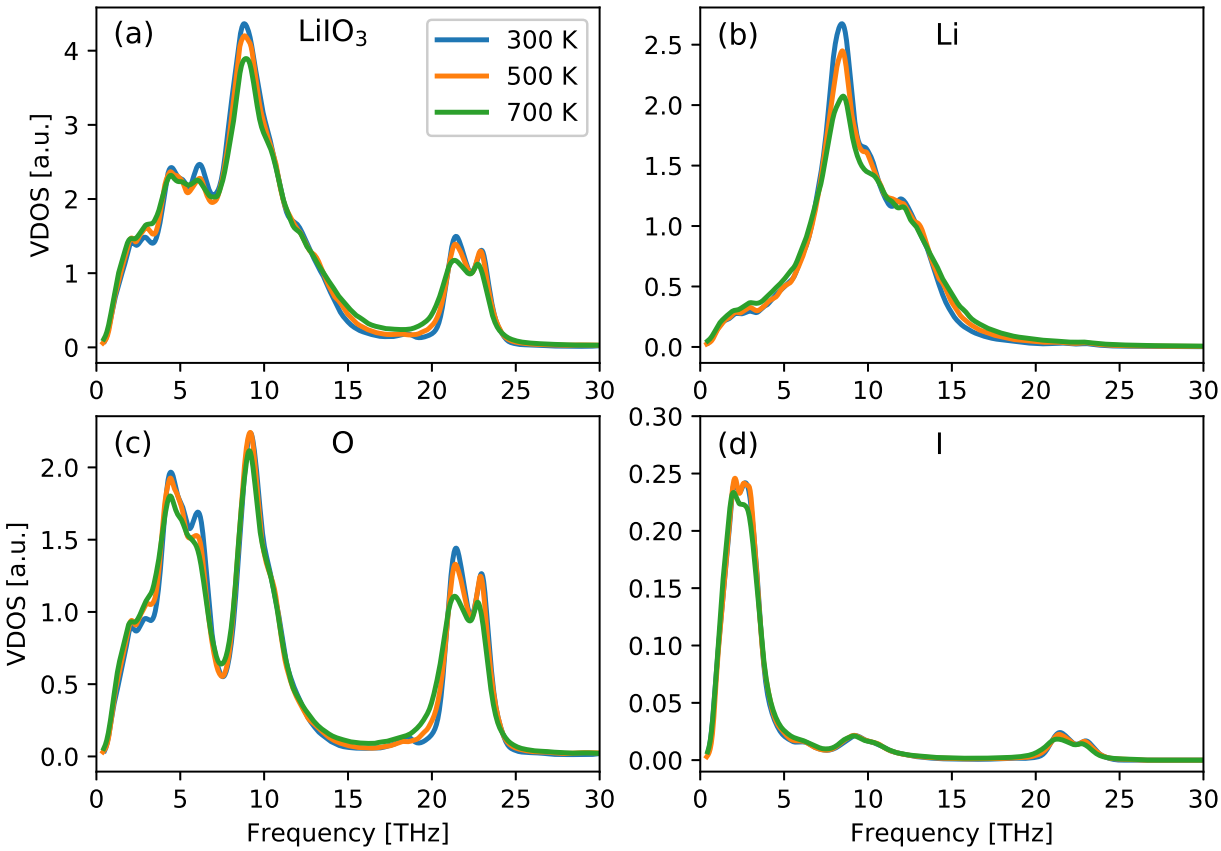

Supplemental Figure 5: Density of vibrational states calculated for non-stoichiometric $LiIO_3$ at different temperatures by considering (a) all the atoms in the system and (b)-(d) each individual species. Results are obtained from the Fourier transform of the velocity-velocity autocorrelation function calculated during long AIMD simulations.

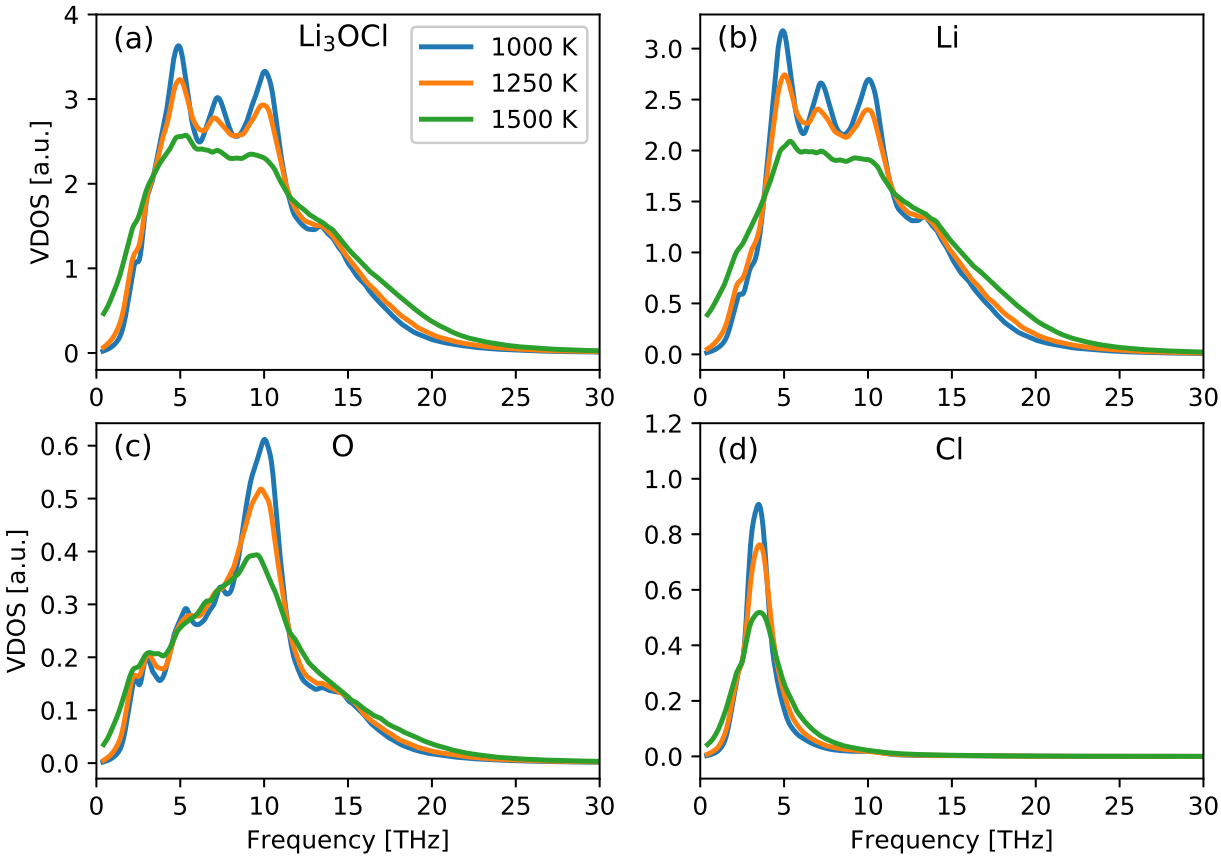

Supplemental Figure 6: Density of vibrational states calculated for non-stoichiometric Li_3OCl at different temperatures by considering (a) all the atoms in the system and (b)-(d) each individual species. Results are obtained from the Fourier transform of the velocity-velocity autocorrelation function calculated during long AIMD simulations.

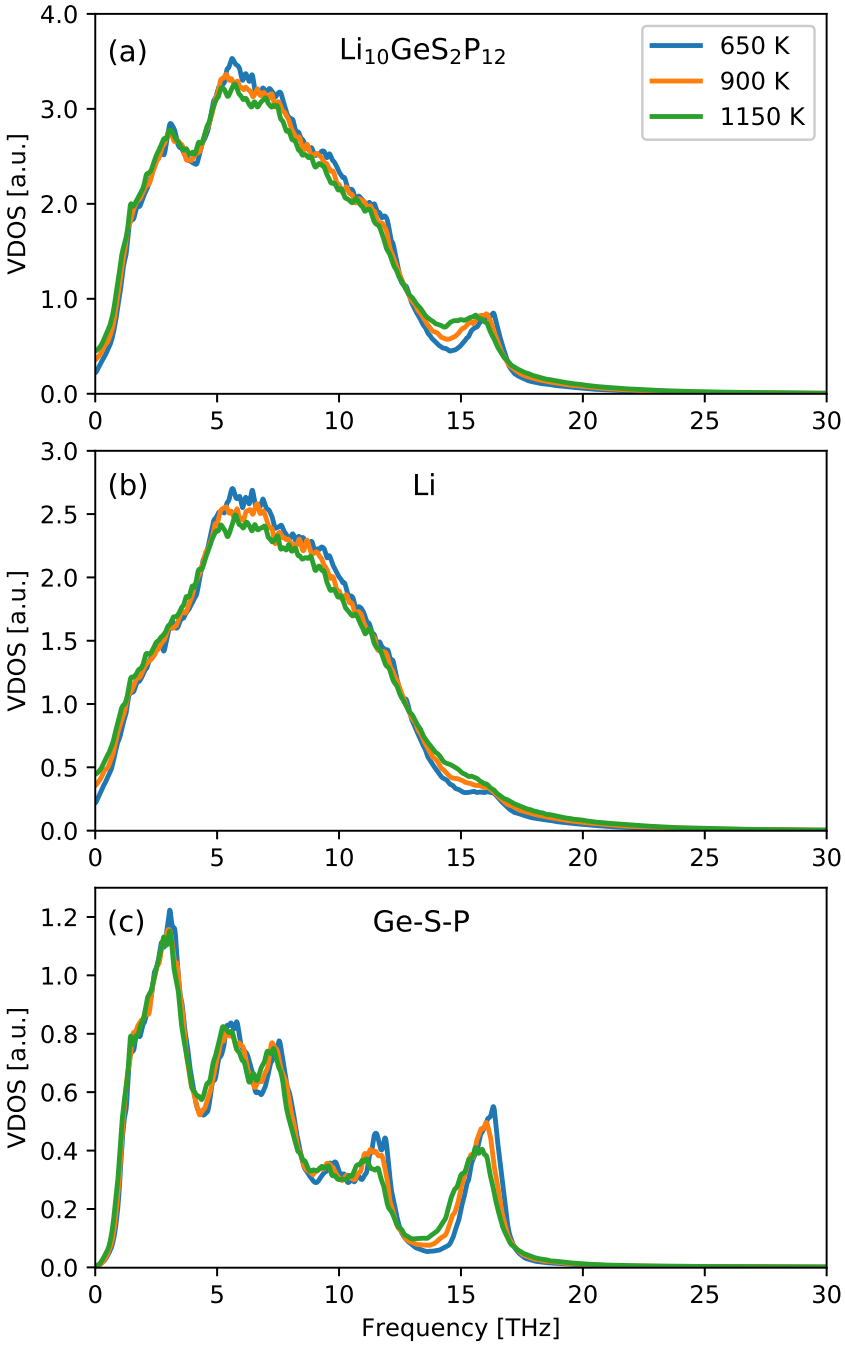

Supplemental Figure 7: Density of vibrational states calculated for non-stoichiometric $Li_{10}GeP_2S_{12}$ at different temperatures by considering (a) all the atoms in the system, (b) Li ions alone, and (c) all species but lithium. Results are obtained from the Fourier transform of the velocity-velocity autocorrelation function calculated during long AIMD simulations.

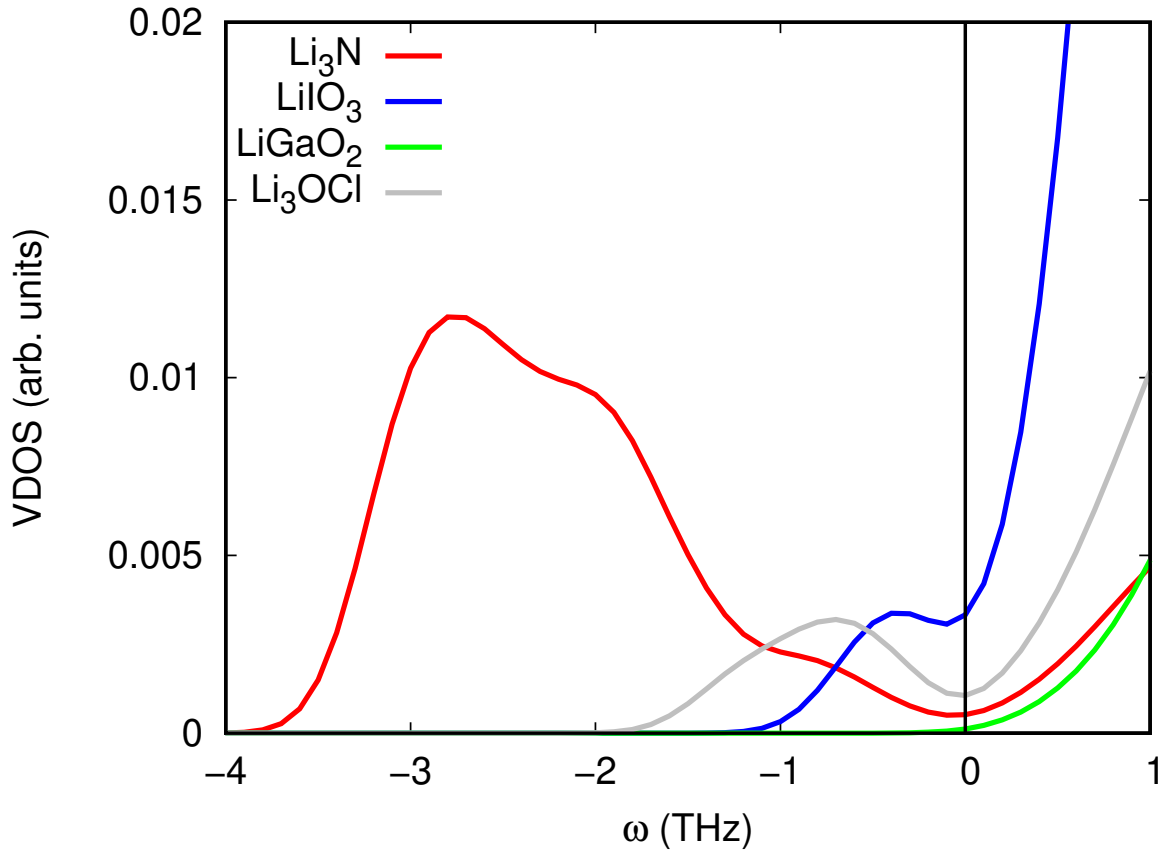

Supplemental Figure 8: Zero-temperature density of vibrational states calculated for non-stoichiometric Li_3OCl, Li_3N, $LiGaO_2$, and $LiIO_3$ with harmonic approaches. All compounds but $LiGaO_2$ display imaginary phonon frequency modes in their VDOS.

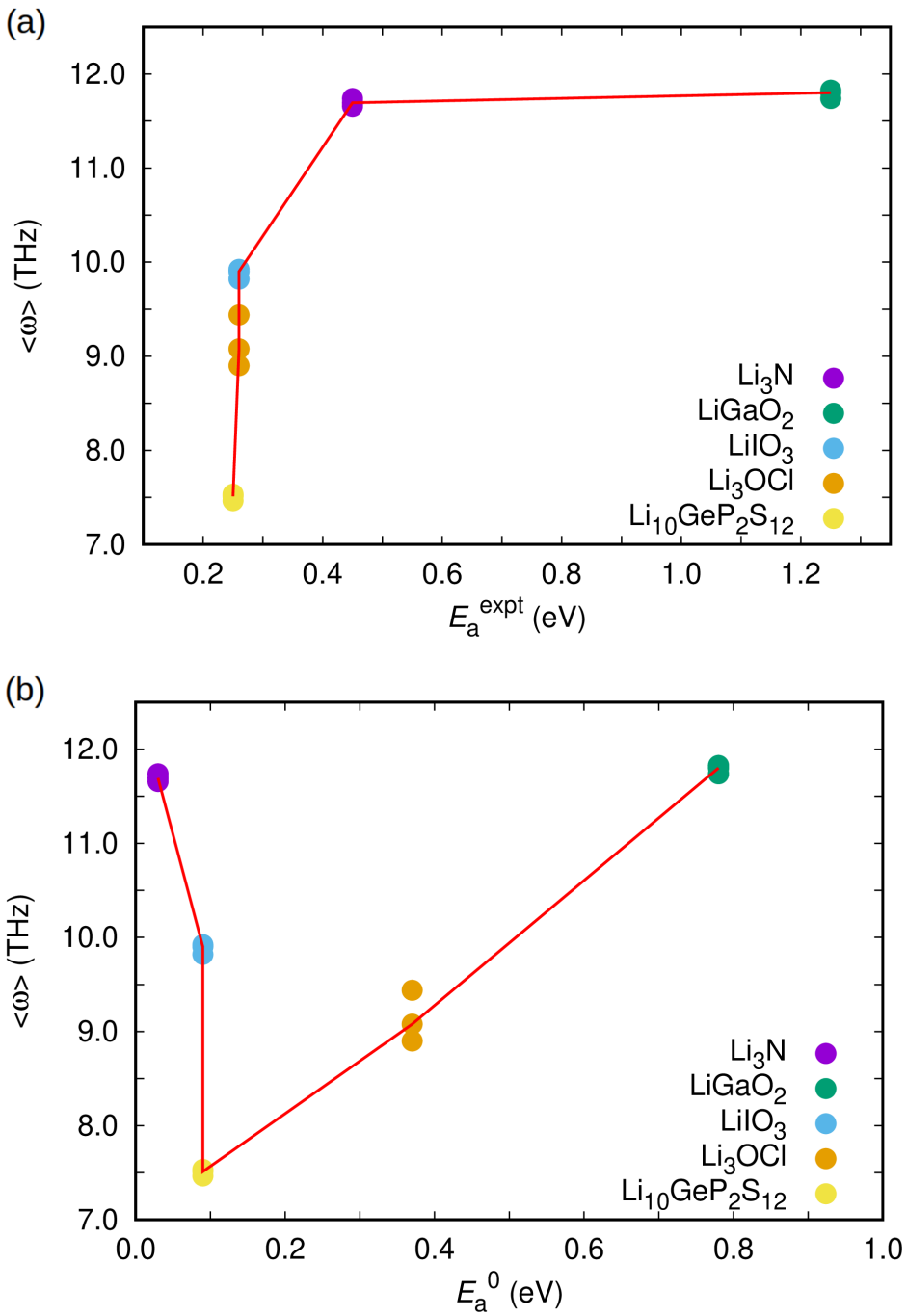

Supplemental Figure 9: Phonon band center versus the activation energy barrier estimated in experiments, E_a^{expt}, and calculated with zero-temperature methods, E_a^0, for ion migration in lithium FIC. A direct correlation between migration activation energies and average phonon frequencies neither can be established in these cases.

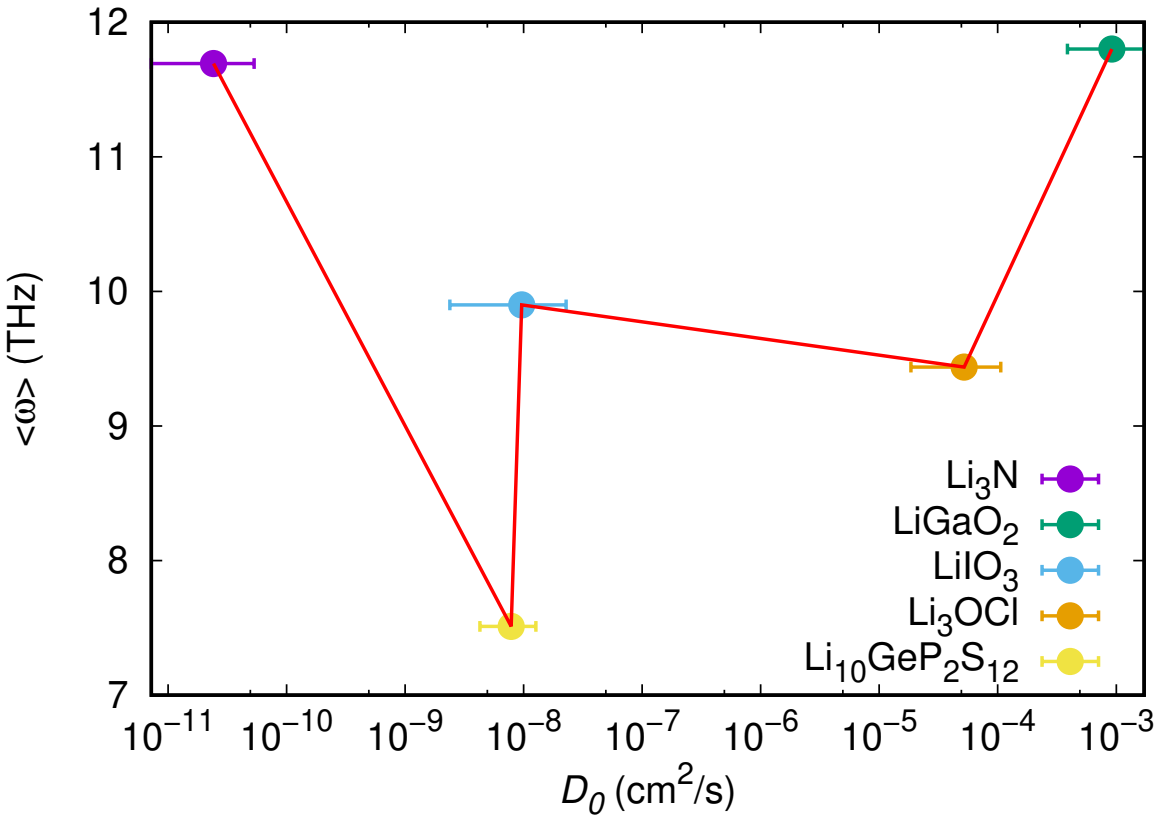

Supplemental Figure 10: Pre-exponential factors represented as a function of the average phonon frequency for the lithium fast-ion conductors considered in our study. None direct correlation between D_0 and $\langle\omega\rangle$ can be established based on our AIMD results. The x-axis is expressed in logarithmic scale.

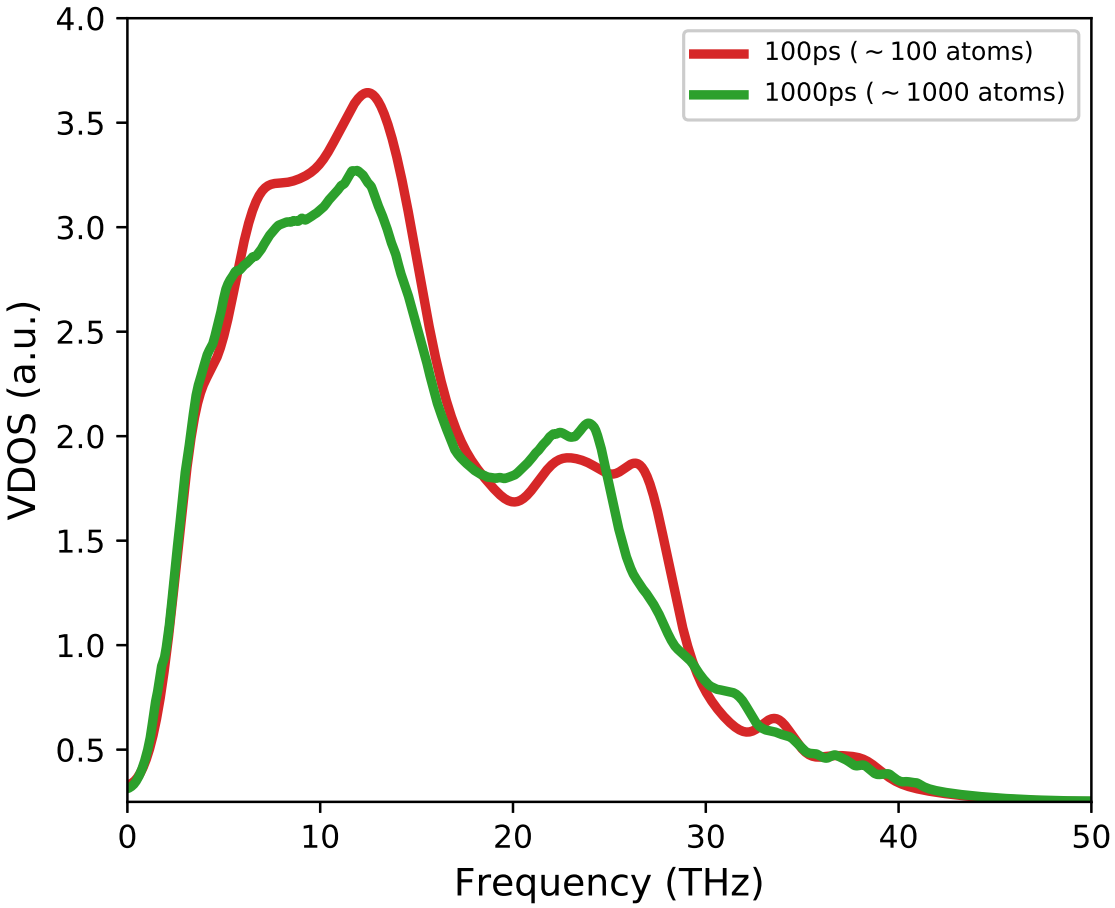

Supplemental Figure 11: Test on the convergence of the calculated VDOS performed for Li_3N by using a classical potential and molecular dynamics. The differences among the VDOS calculated in the 100 atoms–100 ps and 1,000 atoms–1,000 ps cases, although appreciable, lead to small numerical discrepancies of $< 1\%$ in the resulting average phonon frequencies $\langle\omega\rangle$.

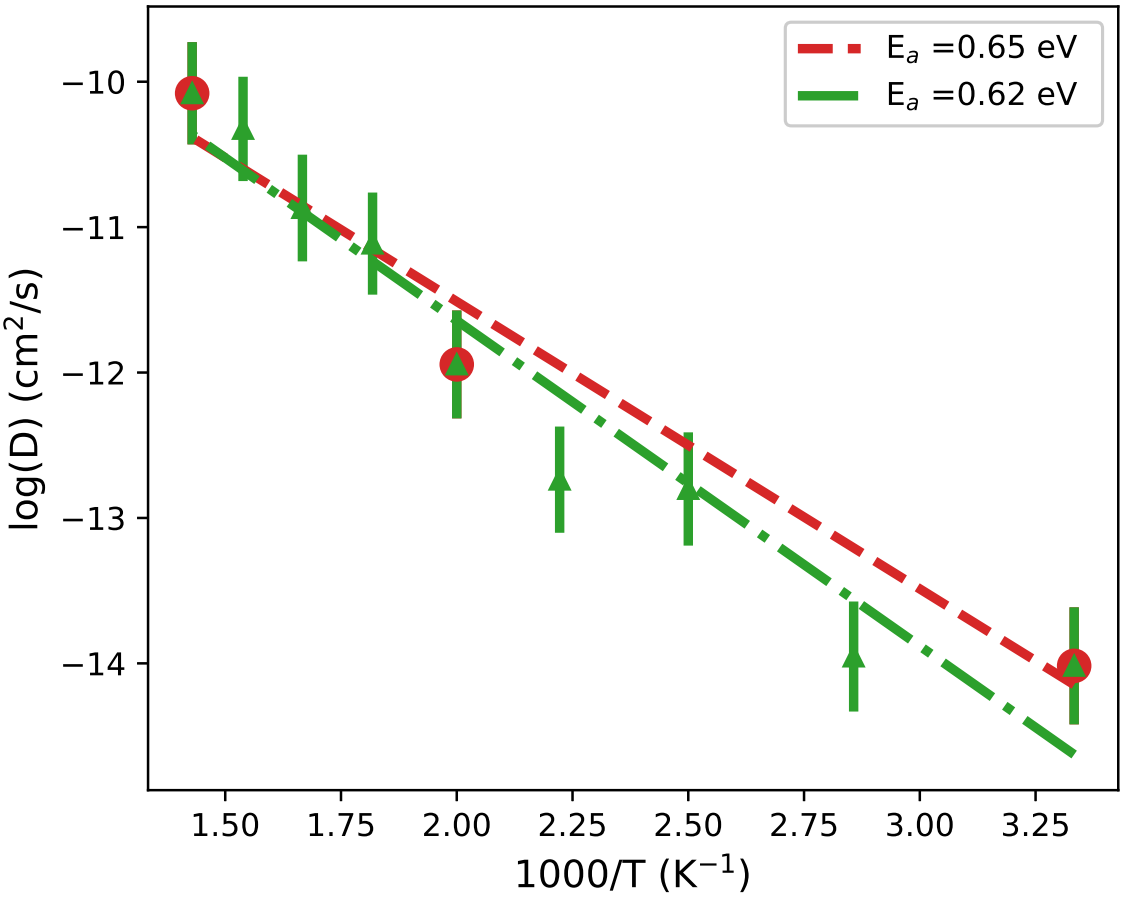

Supplemental Figure 12: Test on the convergence of the estimation of E_a as a function of the number of available D points. Calculations have been peformed for Li_3N by using a classical potential and molecular dynamics. The value of the fitted E_a's obtained with just three or nine D points spaning over the same T-interval, are compatible to within their statistical uncertainties (that is, differ by less than 5%).

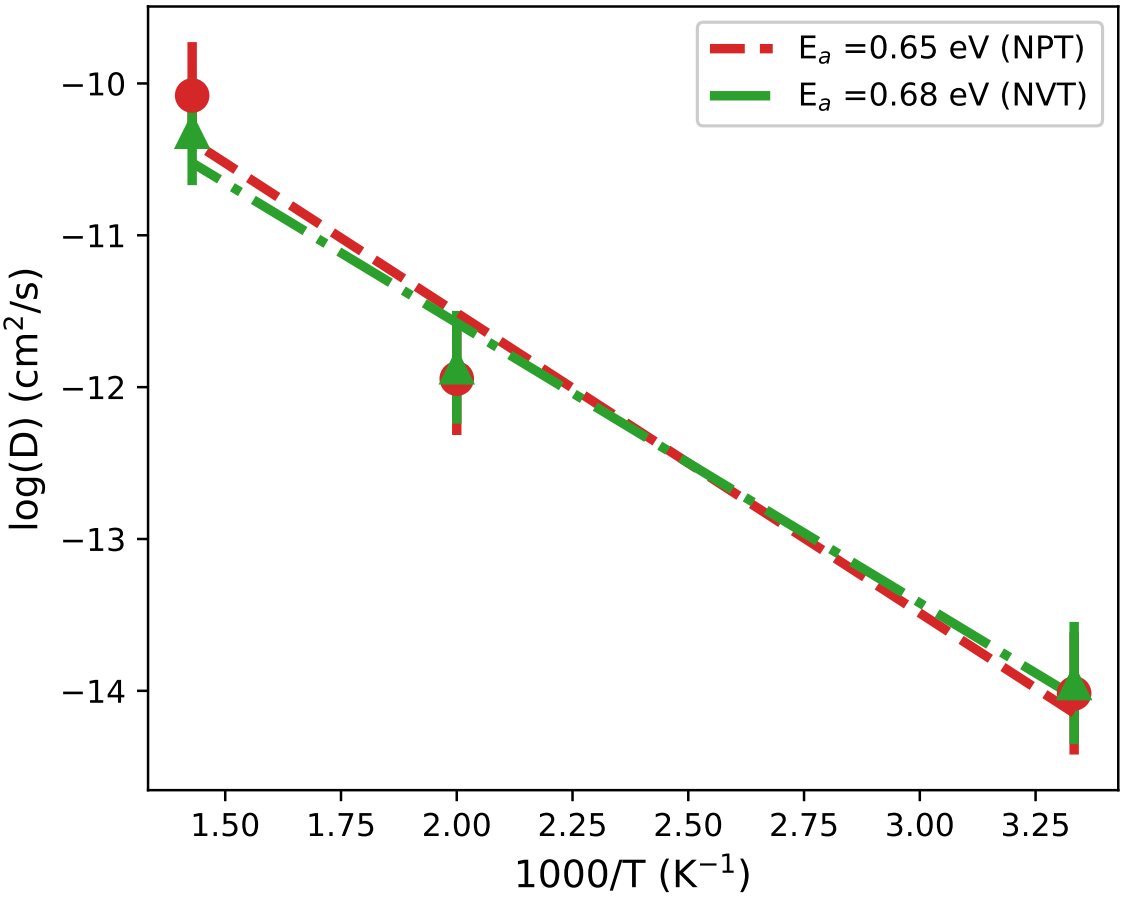

Supplemental Figure 13: Test on the numerical errors affecting E_a as a consequence of the neglection of thermal expansion effects. The volumes in the NVT simulations are constrained to the equilibrium V's determined at zero temperature. Thermal expansion effects are fully taken into account in the NPT simulations. The value of the fitted E_a's obtained in the NVT and NPT simulations are compatible to within 5%.

SUPPLEMENTAL TABLES

τ_{total} (ps)	T_{min}/T_{max} (K)	a (Å)	b (Å)	c (Å)	α (∘)	β (∘)	γ (∘)	c_v (%)	n^o runs (stoi/vac)
				Li_3N					
250	300/900	10.68	10.68	18.97	90	90	120	~ 2	4/4
				$LiGaO_2$					
200	500/1300	10.21	11.00	12.94	90	90	90	~ 2	4/4
				LiF					
250	400/1250	14.84	14.84	11.87	60	60	60	~ 2	5/5
				$LiIO_3$					
200	500/1100	16.57	16.57	15.89	90	90	120	~ 2	4/4
				Li_3OCl					
200	1000/1650	16.30	16.30	16.30	90	90	90	~ 2	4/4
				$Li_{10}GeP_2S_{12}$					
230	650/1400	17.61	17.61	12.70	90	90	90	–	4/0

Supplemental Table I: Additional technical details on our AIMD simulations of Li FIC. τ_{total} represents the total duration of each simulation run, T_{min}/T_{max} the minimum and maximum temperatures considered in our simulations, and $a, b, c, \alpha, \beta, \gamma$ the geometric parameters of the simulation supercells. The concentration of lithium vacancies in the non-stoichiometric systems has been constrained to $\sim 2\%$; the total number of AIMD runs carried out for the stoichiometric ("stoi") and non-stoichiometric ("vac") systems is also specified.

	T_s (K)			
Number of atoms →	$\sim 10^2$	$\sim 10^3$	$\sim 10^4$	$\sim 10^5$
Total time (ps) ↓				
	Li_3N			
$\sim 10^1$	–	1000	1000	1000
$\sim 10^2$	**900**	1000	1000	1000
$\sim 10^3$	1000	1000	1000	**1000**
	Li_3OCl			
$\sim 10^1$	1000	1000	1000	1000
$\sim 10^2$	**1000**	1200	1200	1200
$\sim 10^3$	1000	1200	1200	**1200**

Supplemental Table II: Results of the molecular dynamics tests performed to estimate the finite-size bias affecting the estimation of superionic transition temperatures, T_s, in non-stoichiometric lithium fast-ion conductors (e.g., Li_3N and Li_3OCl). T_s has been chosen arbitrarily as the temperature above which the lithium diffusion coefficient, D, is larger than 10^{-6} cm^2 s^{-1}. The results of our finite-size tests show that by performing dynamical simulations with a number of ions of $N \sim 10^2$ and a total duration time of $t_{\text{total}} \sim 10^2$ ps, one can estimate T_s that are accurate to within $100 - 200$ K (i.e., by regarding the results obtained for $N \sim 10^5$ and $t_{\text{total}} \sim 10^3$ ps as numerically exact).

$\langle\omega\rangle$ (THz)		
Number of atoms $\rightarrow$	$\sim 10^2$	$\sim 10^3$
Total time (ps) $\downarrow$		
$\sim 10^2$	**13.33**	13.39
$\sim 10^3$	13.36	**13.41**

Supplemental Table III: Results of the molecular dynamics tests performed to estimate the finite-size bias affecting the estimation of $\langle\omega\rangle$. Results have been obtained for stoichiometric Li_3N at $T = 1000$ K. The results of our finite-size tests show that by performing dynamical simulations with a number of ions of $N \sim 10^2$ and a total duration time of $t_{\text{total}} \sim 10^2$ ps, one can estimate $\langle\omega\rangle$ that are accurate to within $< 1\%$ (i.e., by regarding the results obtained for $N \sim 10^3$ and $t_{\text{total}} \sim 10^3$ ps as numerically exact).

SUPPLEMENTAL METHODS

Molecular dynamics (MD) (N, P, T) simulations are performed with the LAMMPS code [1] in order to assess the effects of finite-size bias on the estimation of the superionic transition temperature, T_s, and average phonon frequency, $\langle\omega\rangle$, for lithium fast-ion conductors (FIC). The pressure and temperature in the system are kept fluctuating around a set-point value by using thermostatting and barostatting techniques, in which some dynamic variables are coupled to the particle velocities and simulation box dimensions (the external pressure is always fixed to zero). The interactions between the ions are modeled with the rigid-ion Born-Mayer-Huggins potentials employed previously in works [2] (for Li_3N) and [3] (for Li_3OCl). We use simulation boxes containing from 100 up to $100,000$ atoms, and apply periodic boundary conditions along the three Cartesian directions. Newton's equations of motion are integrated by means of the usual Verlet's algorithm with a time-step length of 10^{-3} ps. The total duration of the MD runs varies from 10 up to $1,000$ ps. A particle-particle particle-mesh k-space solver is used to compute long-range van der Waals and Coulomb interactions beyond a cut-off distance of 12 Å at each time step.

Although we appreciate some differences between the T_s and $\langle\omega\rangle$ values obtained with classical potentials and density functional theory, we assume that finite-size errors affect in a very similar manner both series of results. For this reason and because the computational load associated to first-principles simulations is quite high, we have performed our finite-size bias tests at the classical-potential level. The results of our MD tests are summarised in Supplementary Tables 2 and 3. Supplementary Table 2 shows that by using simulation cells containing hundreds of ions, $N \sim 10^2$, and considering a total simulation time of hundreds of picoseconds, $t_{\text{total}} \sim 10^2$ ps, one can estimate accurate superionic transition temperatures that are exact to within $100 - 200$ K (we note that the results obtained for $N \sim 10^5$ and $t_{\text{total}} \sim 10^3$ ps are regarded as numerically exact since they appear to be perfectly converged). Likewise, lithium diffusion coefficients are estimated very accurately (i.e., to within 3%) since T_s is identified with the temperature at which $D \sim 10^{-6}$ cm^2 s^{-1}. Supplementary Table 3 shows that by using simulation cells containing hundreds of ions, $N \sim 10^2$, and considering a total simulation time of hundreds of picoseconds, $t_{\text{total}} \sim 10^2$ ps, one can estimate average phonon frequencies that are accurate to within $< 1\%$ (the VDOS results obtained for $N \sim 10^3$ and $t_{\text{total}} \sim 10^3$ ps are regarded as numerically exact). Supplementary

Fig.11 explicitly shows the VDOS differences obtained for two 100 ps–100 ions and 1,000 ps–1,000 ions MD runs, which can be regarded as reasonably small.

Ab initio molecular dynamics (AIMD) simulations are computationally quite expensive. Consequently, in this work (where we have analysed up to 6 different lithium FIC under broad composition and temperature conditions, see Supplementary Table 1) we have typically employed three D points to estimate lithium activation energy barriers, E_a, and diffusivity pre-exponential factors, D_0, by means of exponential fits. In addition, we have neglected thermal expansion effects since the volume of the systems have been constrained to their equilibrium values obtained at zero temperature. We have performed a series of numerical tests at the force-field level, which is computationally affordable, to assess how those two approximations affect the accuracy in our first-principles results reported in the main text. Supplementary Fig.12 and Supplementary Fig.13 enclose the results of those tests, which have been carried out for Li_3N with the same rigid-ion Born-Mayer-Huggins potential model than specified above. We may conclude that the numerical uncertainties in E_a caused by considering three D points in the exponential fits and the neglection of thermal expansion are below 5%, which are of the same order of magnitude than already reported in Table 1 in the main text.

In view of the finite-size error and other numerical tests presented in this section, we may conclude that the D, E_a, D_0, and $\langle\omega\rangle$ results that have obtained with AIMD techniques and are reported in the main text can be regarded as reliable and accurate (e.g., involve simulation boxes containing $N \sim 10^2$ ions and total simulation times of $t_{\text{total}} \sim 10^2$ ps). Therefore, as we mentioned in the Introduction section in the main text, realistic AIMD simulation of lithium fast-ion materials, typically referred to as type-II [4,5], nowadays is within reach.

SUPPLEMENTAL REFERENCES

[1] J. S. Plimpton, J. Comp. Phys. **117**, 1 (1995) *http://lammps.sandia.gov*.

[2] A. K. Sagotra, D. Chu, and C. Cazorla, Nat. Commun. **9**, 3337 (2018).

[3] A. K. Sagotra, D. Errandonea, and C. Cazorla, Nat. Commun. **8**, 963 (2017).

[4] S. Hull, Rep. Prog. Phys. **67**, 1233 (2004).

[5] C. Cazorla and D. Errandonea, Phys. Rev. B **98**, 186101 (2018).